

## FULL ARTICLE

# Superficial photothermal laser ablation of ex vivo sheep esophagus using a cone-shaped optical fiber tip

Serhat Tozburun<sup>1,2,3\*</sup> 

<sup>1</sup>Izmir Biomedicine and Genome Center, Izmir, Turkey

<sup>2</sup>Izmir International Biomedicine and Genome Institute, Dokuz Eylul University, Izmir, Turkey

<sup>3</sup>Department of Biophysics, Faculty of Medicine, Dokuz Eylul University, Izmir, Turkey

### \*Correspondence

Serhat Tozburun, Izmir Biomedicine and Genome Center, Dokuz Eylul University Health Campus, Mithatpasa Ave. 58/5 35330 Izmir, Turkey.

Email: serhat.tozburun@ibg.edu.tr

### Funding information

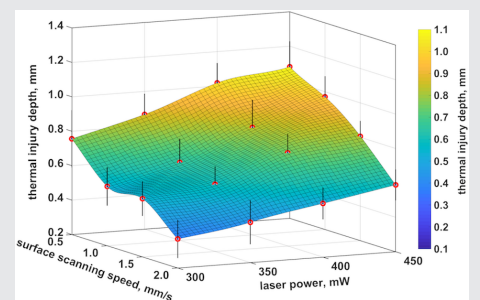
H2020 Marie Skłodowska-Curie Actions, Grant/Award Number: 835907; Scientific and Technology Research Council of Turkey (TÜBİTAK), Grant/Award Number: 117E985; Turkish Academy of Sciences Young Scientists Award Programme, Grant/Award Number: 2018 TÜBA-GEBİP; European Union's Horizon 2020 Research

### Abstract

Superficial photothermal laser ablation (SPLA) may be useful as a therapeutic approach producing a depth of injury that is sufficient to eliminate mucosal lesion but not deep enough to induce thermal effects in deeper tissue layers. The purpose of this preliminary study is twofold: (a) to describe design steps of a fiber probe capable of delivering a tightly focused laser beam, including Monte-Carlo-based simulations, and (b) to complete the initial testing of the probe in a sheep esophagus model, ex vivo. The cone-shaped (tapered) fiber tip was obtained by chemical etching of the optical fiber. A 1505 nm diode laser providing power up to 500 mW was operated in continuous wave. The successful SPLA of the sheep mucosa layer was demonstrated for various speed-power combinations, including 300 mW laser power at a surface scanning rate of 0.5 mm/s and 450 mW laser power at a surface scanning rate of 2.0 mm/s. Upon further development, this probe may be useful for endoscopic photothermal laser ablation of the mucosa layer using relatively low laser power.

### KEYWORDS

chemical etching, fiber probe, Monte Carlo, mucosa, photothermal ablation



## 1 | INTRODUCTION

Gastrointestinal tract diseases, such as esophageal cancer, colon cancer, or rectal cancer, can be caused by precancerous superficial mucosal lesions and may then spread to deep tissue structures. For example, Barrett's esophagus (BE) is a precancerous condition of esophagus [1, 2] and is associated with esophageal adenocarcinoma [3]. BE appears as an inflammatory consequence of the

esophageal lining resulting from chronic reflux of acid. This is a metaplastic change of the esophageal epithelium from squamous to columnar type epithelium. The incidence of esophageal carcinoma has increased approximately sixfold over the past two decades and making it the eighth common incident cancer in the world [3–5]. It has been reported that the BE prevalence in patients with gastro esophageal reflux disease varies between 1.3% and 4.05% in Europe [6, 7]. Prospective

This is an open access article under the terms of the Creative Commons Attribution License, which permits use, distribution and reproduction in any medium, provided the original work is properly cited.

© 2020 The Author. *Journal of Biophotonics* published by WILEY-VCH Verlag GmbH & Co. KGaA, Weinheim

studies of up to 1000 patients have shown that the prevalence of BE in Turkey was 1.5% [8, 9].

Medication is a traditional treatment strategy of the BE. This drug therapy method aims to aggressively reduce acid production in patients having gastroesophageal reflux disease with BE [10, 11]. Although this method typically prevents further damage to the esophagus lining caused by acid reflux, it does not necessarily heal existing damage or eradicate the abnormal lining. Therefore, endoscopic treatment approaches have been developed for the treatment of existing mucosal lesions. One of these is the endoscopic mucosal resection technique relies on lifting mucosal lesion from the deeper layers by liquid injection. The lesion tissue is then mechanically resected and removed. However, this technique is generally used for the treatment of mucosal lesions smaller than 2 cm in length [12–14]. In addition to the mucosal resection technique, endoscopic thermal ablation is another approach that is considered a suitable treatment method for BE patients. This method is the process of heating the target mucosa layer with absorbed energy. Radiofrequency (RF) ablation is a common endoscopic thermal ablation treatment [15–18]. Here, an endoscopic device containing the electrodes is placed next to the mucosal lining, and provides a local heat field to eliminate the abnormal tissue of the esophagus. Another method of ablation is endoscopic photothermal mucosa ablation, which uses laser radiation to deliver heat energy to the mucosa tissue [19–21]. The essential mechanism in this method is to match the laser wavelength and the corresponding optical penetration depth to the therapeutic depth in the targeted layer.

However, although endoscopic therapy interventions attempt to effectively reverse BE and reduce relative mortality from esophageal cancer, the main challenge associated with the current deployments of both RF ablation and photothermal laser ablation is that the depth of treatment typically has a deeper thermal injury than the mucosa layer [3, 7]. This therapeutic failure can thermally damage deeper layers that are not primarily intended. Even worse, multiple treatment sessions with this possible thermal damage cause organ narrowing, bleeding or perforation [12, 18, 20]. To address this challenge, approaches that specifically apply a confined depth of thermal effect on the epithelial layer of  $\sim 500\ \mu\text{m}$  thickness [22] are expressly intended. However, for example, commercially available endoscopy systems employing RF ablation (ie, the most commonly used method of BE treatment because of its high efficacy and relatively minimally invasive nature) provide thermal damage depth of  $>800\ \mu\text{m}$  [22]. This depth of thermal effect may not be shallow enough to prevent residual thermal damage to the deep tissue layers in some cases. Therefore, the

availability of effective endoscopic approaches with limited thermal therapeutic effects on the epithelium layer is still of interest in the treatment of BE.

In this preliminary study, we investigate a cone-shaped fiber probe that delivers a focused Gaussian laser beam with relatively low laser power for superficial photothermal laser ablation (SPLA) of the mucosa layer. Wet chemical etching of the distal fiber tip results in a cone-shaped fiber tip capable of delivering a  $>4\text{-}\mu\text{m}$ -diameter ( $1/e^2$ ) laser beam. In an ex vivo sheep esophagus model, a single-session photothermal ablation using a cone-shaped fiber probe is successfully observed in epithelium and submucosa layers. Two computer simulations are complementary parts of the preliminary study. Beam propagation simulations aim to roughly estimate the tight focus of the laser beam produced by a cone-shaped fiber probe and the diameter of the laser beam at the focal point. Photothermal laser ablation simulations aim to analyze the cone-shaped fiber probe induced injury depth as a function of the surface scanning speed and the laser power of the probe on the esophageal surface. Section 2 begins with a description of the acid etching process (Section 2.1). Next, computer modeling developed to mimic the photothermal dynamics of the probe is detailed (Section 2.2). ex vivo tissue study is described in Section 2.3. The performance of the fiber probe for the SPLA of ex vivo sheep esophagus is summarized in Section 3. Finally, Section 4 discusses the current limitations of the study and summarizes the study.

## 2 | EXPERIMENTAL

### 2.1 | Wet chemical etching

In photothermal mucosal ablation studies, infrared (IR) laser radiation (1505 nm) was coupled to a probe using a cone-shaped optical fiber (8.2- $\mu\text{m}$  Ge-doped silica

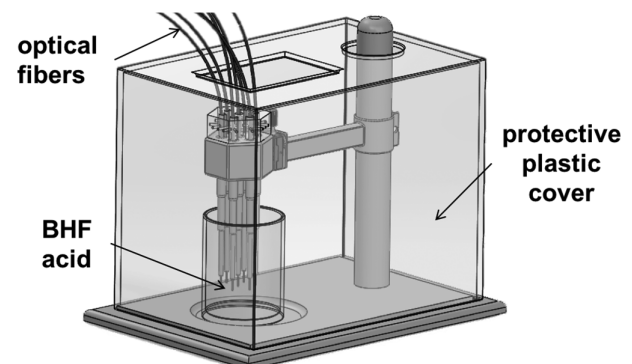


**FIGURE 1** Representative illustration of the experimental setup for buffered hydrofluoric (BHF) acid etching of optical fibers

core with 125- $\mu\text{m}$  pure silica cladding). The fiber tip was modified by wet chemical etching/meniscus etching, which offered a simple mechanism for tapering fiber tips with a less expensive experimental setup. In this technique [23, 24], as the radius of the fiber decreases, the height of the meniscus profile formed between the optical fiber and the etchant material gradually decreases due to the surface tension. This process continues until the fiber, etchant and oil meniscus interface region breaks away from the tip of the fiber.

A schematic illustration of the experimental setup, used for chemical etching studies with an 8.2- $\mu\text{m}$ -core optical fiber, is shown in Figure 1. The fiber tips were stripped to a length of 3.5 mm and cleaved by using a fiber cleaver. The core of the distal fiber tip was etched with buffered hydrofluoric (BHF) acid (J. T. Baker, Philips) for 90 minutes at room temperature and then the etched fibers were cleaned thoroughly in distilled (DI) water. During the etching process, the fiber was surrounded by 49% HF acid diluted with DI water in the ratio 1:4 (acid/water). A small amount of toluene, which covered the free surface of the acid, was added to prevent evaporation of the dilute acid.

## 2.2 | Photothermal mucosa ablation simulations

To analyze the thermal injury depth as a function of laser power induced by the cone-shaped fiber probe, computer simulations and damage calculations were performed. Besides, the optimal scanning speed of the probe along the esophageal surface was examined for adequate SPLA.

Simulation studies consisted of three main steps (Figure 2). First, the Monte Carlo method [25] was employed to determine the distribution of photons in tissue as a function of wavelength-dependent parameters (ie,

absorption, scattering, and anisotropy factor). In this method, a statistical random walk approach was used to model the propagation of light in the medium. Step size was randomly sampled according to the optical properties of the tissue model. The target tissue was defined by tissue thickness ( $t$ , mm), and wavelength-dependent parameters: Refractive index ( $n$ ), scattering coefficient ( $\mu_s$ ,  $\text{cm}^{-1}$ ), absorption coefficient ( $\mu_a$ ,  $\text{cm}^{-1}$ ) and anisotropy factor ( $g$ ).

In the second step, the calculated photon distribution profile was used as a heat source in a time-dependent model of heat diffusion. The thermal behavior was based on Pennes' bioheat equation:

$$\rho C \frac{\partial T}{\partial t} = \nabla \cdot (k \nabla T) + q, \quad (1)$$

where  $\rho$ ,  $C$ ,  $k$ ,  $q$ , and  $T$  are the local tissue density ( $\text{kg/m}^3$ ), specific heat ( $\text{J kg}^{-1} \text{ } ^\circ\text{C}$ ), thermal conductivity ( $\text{W m}^{-1} \text{ } ^\circ\text{C}$ ), the thermal source of the laser irradiation (computed by Monte Carlo) and the resulting tissue temperature in a function of space and time, respectively. The finite-element method solved this partial differential equation over time and space. The solution was performed on MATLAB's built-in PDE Toolbox (MathWorks, Inc.). Finally, the thermal injury was computed in the third step using Arrhenius damage integral [26] to generate the damage index followed by a normalization factor, which represented the fraction of coagulated proteins in a given volume. The thermal injury parameter  $\Omega(x,y,z,t)$  depended exponentially on temperature and linearly on heating time,

$$\Omega(x,y,z,t) = \Lambda \int_0^\tau \exp\left(-\frac{E_a}{RT(x,y,z,t)}\right) dt, \quad (2)$$

where  $\Lambda$  ( $\text{s}^{-1}$ ) is a frequency factor;  $\tau$  (s) is the total heating time (the total exposure time);  $E_a$  (J/mol) is an activation

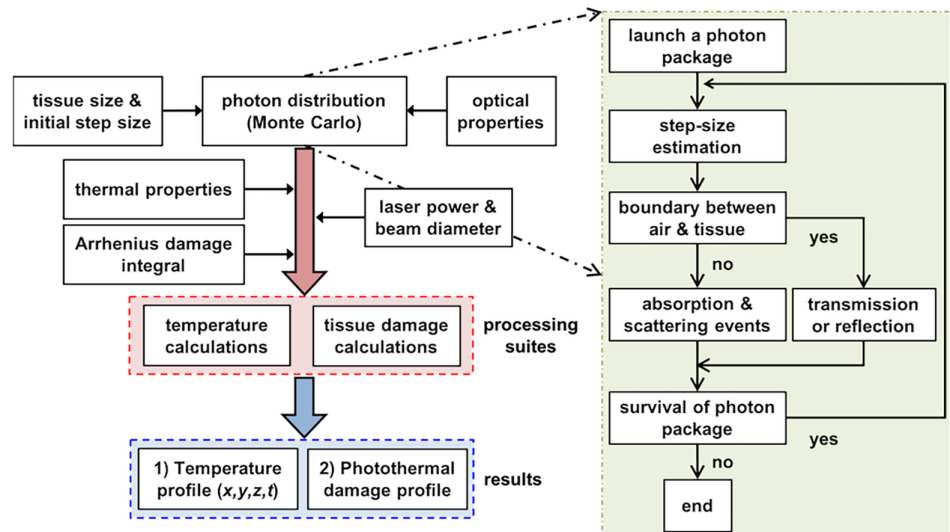


**FIGURE 2** A flow block diagram of the developed computer model

energy of the transformation;  $R$  ( $8.314 \text{ J K}^{-1} \text{ mol}^{-1}$ ) is the universal gas constant; and  $T(x,y,z,t)$  is the absolute temperature of the tissue in degrees Kelvin. Numerical values of frequency factor ( $\Lambda$ ) and activation energy ( $E_a$ , corresponding to the minimum amount of energy required to initiate the transformation process) were estimated from the literature.

The thermal injury was expressed as damage probability given by:

$$\text{Damage}(\%) = 100(1 - \exp(-\Omega(x,y,z,t))). \quad (3)$$

The damage integral was normalized to be 1 for producing the damage index, or so-called the damage probability. The index was calculated to be 0% for a damage parameter of 0, 63% for a damage parameter of 1, and 99% for a damage parameter of 4.6, associated with the protein deterioration index of the biological structures in the unit volume.

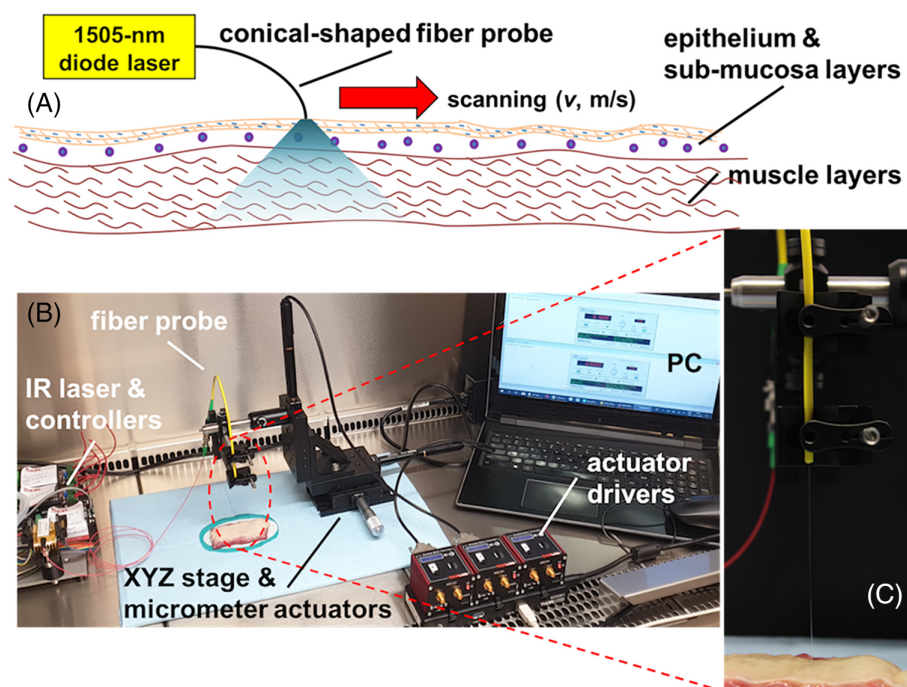
## 2.3 | Ex vivo tissue studies

Figure 3 shows a schematic diagram and pictures of the experimental setup used for photothermal ablation, ex vivo. Sheep esophagus was chosen as an animal model due to its similarity to the human esophagus in terms of morphology and layer thickness [27–30]. All ex vivo esophageal studies were performed in a fume hood (Köttermann, Germany) providing a biologically safe environment under a protocol approved by the Biosafety Committee at the Izmir Biomedicine and Genome Center.

A single-mode, pigtailed, diode laser (QPC Lasers Inc., Sylmar, California) emitting laser power up to 500 mW at a wavelength of 1505 nm was used as an IR light source in the system. Laser radiation at 1505 nm has an optical penetration depth of  $>0.57 \text{ mm}$  in water [31], the primary chromophore for soft tissues in the near-IR spectrum.

An XYZ linear translation optomechanical stage was employed in ex vivo studies (Figure 3B). With the same type of motorized micrometer actuators (Z812; Thorlabs, Newton, New Jersey), the two axes of the stage allowed perfect control of the probe parallel and perpendicular across the tissue surface, respectively. The parallel axis actuator provided a scanning speed of up to 2.5 mm/s with a maximum travel length of 25 mm. In this way, the surface scanning speed was set at a constant value. Furthermore, the perpendicular axis actuator precisely adjusted the distance between the fiber probe tip and the tissue surface with a step size of  $0.4 \mu\text{m}$ . The third axis of the plate was controlled by a manual micrometer actuator (150-801ME; Thorlabs) to align the probe at a resolution of  $10 \mu\text{m}$  on the surface.

Histological examination is the gold standard way of determining the depth of injury by identifying morphological changes in the context of assessing the response to photothermal mucosa ablation. Therefore, tissue samples were collected for histology after esophageal ablation in an ex vivo sheep model. The collected specimens were embedded in a gel compound called optimal cutting temperature and refrigerated at  $-80^\circ\text{C}$ . Then, the region of interest was sectioned from the frozen blocks at a



**FIGURE 3** Experimental setup using chemically etched fiber optics for superficial photothermal laser ablation: Schematic, A, photograph of the setup including the XYZ linear translation optomechanical stage for precise control of the fiber probe along the ex vivo tissue surface, B, close view of the optical fiber probe, C

thickness of  $12\ \mu\text{m}$  for histological processing. Nitroblue tetrazolium chloride (NBT) staining was used to histologically analyze the extent of cellular thermal damage to the esophagus. This staining was active for the cytoplasmic marker enzyme lactate, showing dark blue coloration. In contrast, laser-induced cellular damaged areas did not show blue staining but associated with classical histology.

### 3 | RESULTS

This section quantifies the chemical etching of a single-mode optical fiber, including beam propagation simulations. There is then a series of studies demonstrating the capability of the cone-shaped fiber end in the SPLA. These studies comprise computer simulations based on the Monte Carlo method, *ex vivo* sheep esophagus experiments, and histology analysis.

#### 3.1 | Cone-shaped fiber probe

Figure 4 shows the fiber tip under magnification after chemical etching of the single-mode fiber ( $8.2\ \mu\text{m}$  in core diameter and  $125\ \mu\text{m}$  in cladding diameter). Since the height of the meniscus profile gradually decreased as a function of the contact angle at the interface point, a cone form was obtained by chemical etching at the fiber tip. The height of the cone was  $\sim 260\ \mu\text{m}$ . The chemical etching rate with diluted BHF acid (49%) solution in the ratio of 1:4 (acid/DI water) was estimated to be  $23\ 635\ \mu\text{m}^3/\text{min}$ .

To visualize the fast focusing provided by a cone-shaped fiber probe, computer simulations were performed employing commercially available software (RSoft Photonics, BeamPROP, Version 8.0.1) based on finite difference beam propagation method. These simulations also aimed to roughly estimate the length of the focal point and the diameter of the laser beam at the focus. As shown in Figure 5A, the cone-shaped fiber tip

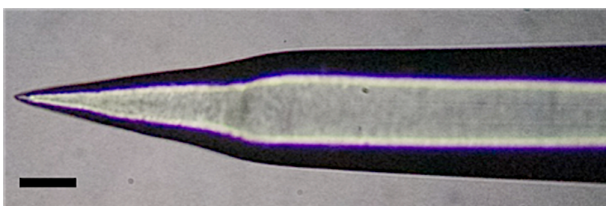


**FIGURE 4** Photograph of the chemically etched single-mode fiber distal tip (scale bar =  $50\ \mu\text{m}$ ). The cone was measured  $\sim 260\ \mu\text{m}$  height for an etching time of 90 minutes

was mimicked with a perfect pyramid structure for beam propagation simulations. The fiber probe was defined by refractive indices of 1.44 for the core and 1.4112 for the cladding [32]. The grid size used in the calculations was set to  $1\ \mu\text{m}$ , and the monitor grid size was  $10\ \mu\text{m}$  to display the results as 2D and 3D color-coded contour maps. The length of the cone-shaped fiber tip was set to  $260\ \mu\text{m}$ , while the total length of the fiber was  $1.6\ \text{mm}$ . The cladding diameter of the fiber was  $125\ \mu\text{m}$ .

Figure 5 presents the results of beam propagation simulations in 2D (Panel B) and 3D (Panel C) formats, respectively. The simulation launched a Gaussian field and propagated the field through the fiber structure along the z-axis. The launch field excited the fundamental mode of the waveguide. After the  $1505\ \text{nm}$  laser radiation propagated through the chemically etched cone-shaped

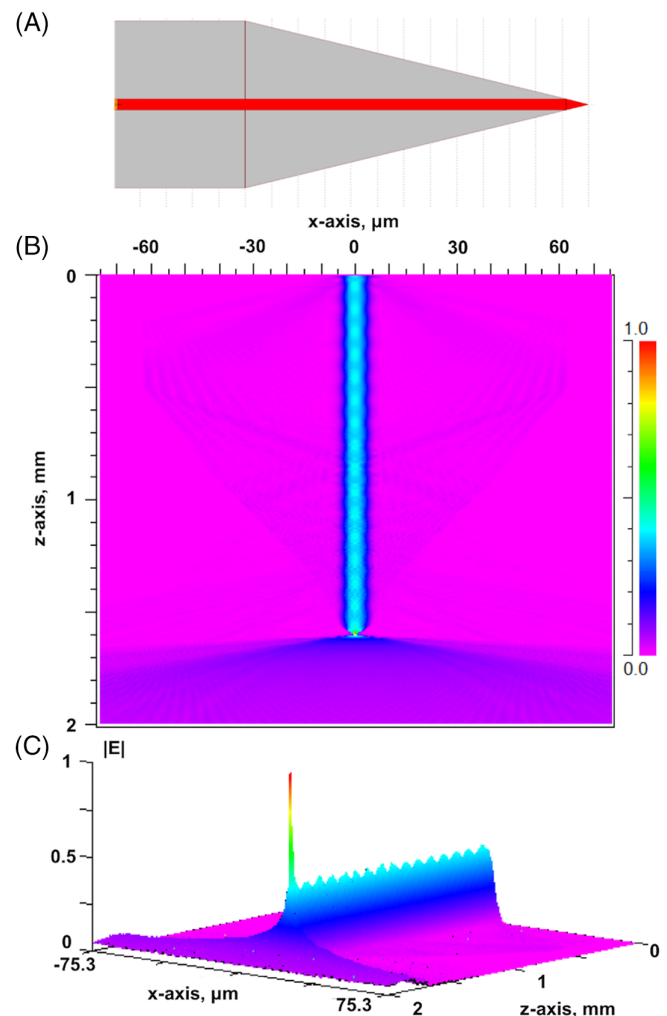


**FIGURE 5** Geometry of the cone-shaped fiber tip used in beam propagation computer simulations, A. Simulation solutions based on the amplitude of the electric field in 2D, B, and 3D, C, formats showing the rapid focus of the infrared (IR) laser beam after passing through a cone-shaped fiber tip

fiber tip, the Gaussian laser beam was focused on a very narrow spot over a distance of approximately  $40\ \mu\text{m}$  ( $23.1\ \mu\text{m} \pm 16\ \mu\text{m}$ ) in free space. The calculated optical intensity distribution at the focus is shown in Figure 6. The  $1/e^2$  width of the light beam was simulated to be  $\sim 3.71\ \mu\text{m}$ . The monitor output was adjusted to show the amplitude of the electric field ( $V/m$ ) normalized to 1 and marked with a color bar.

It should be noted that beam propagation simulations did not take into account the curvature of the fiber probe tip in the calculations because of the lack of extracting the precise value of the curvature. However, as the radius of curvature increases, the working distance (ie, depth defined as the gap between the fiber tip and the focal point having the maximum intensity) increases. Therefore, the working distance and the corresponding laser beam diameter may vary in the case of the experiment. Besides, the beam diameter can be calculated from the diffraction-limited beam focusing model. In this calculation, the beam diameter was calculated as  $4.24\ \mu\text{m}$  at  $1/e^2$  using an estimated focal length of  $23.1\ \mu\text{m}$  as input.

### 3.2 | Photothermal ablation simulations

In the Monte-Carlo study of photothermal mucosal ablation simulations, a uniform 3D grid system of  $1500 \times 1500 \times 900$  defined the esophageal tissue model to estimate photon weight distribution. A volume with a grid size of  $2\ \mu\text{m}$  in all dimensions corresponded to a tissue size of  $4\ \text{mm}$  (x-axis)  $\times$   $4\ \text{mm}$  (y-axis)  $\times$   $1.8\ \text{mm}$  (z-axis, depth in tissue). For tissue temperature and corresponding thermal damage calculations, an esophageal tissue model with a uniform 3D grid system of  $300 \times 300 \times 180$  with a grid size of  $10\ \mu\text{m}$  of each dimension was used. The depth of the modeled tissue was

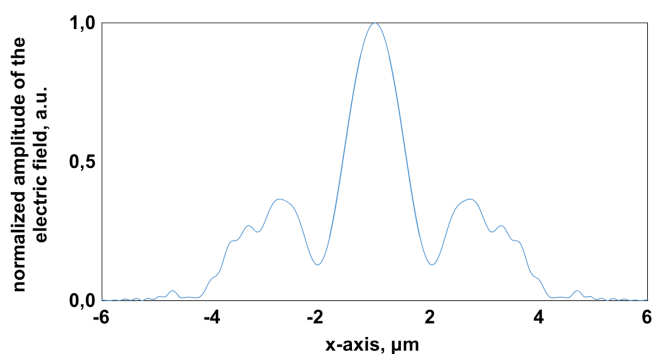


**FIGURE 6** Estimated spatial beam profile at a distance of  $23.1\ \mu\text{m}$  from the tip of the chemically etched fiber. The beam diameter at the level of  $1/e^2$  was calculated to be approximately  $4.3\ \mu\text{m}$

determined by the sum of mucosa layer thickness ( $0.54\ \text{mm}$ ), submucosa layer thickness ( $0.55\ \text{mm}$ ), and muscularis layer thickness ( $0.63\ \text{mm}$ ) [33]. Thermal properties of the tissue and optical properties at a wavelength of  $1.5\ \mu\text{m}$  have been compiled from the literature. Table 1 summarizes all these parameters used in the simulations.

The Monte Carlo-based model was developed in the C programming language; all other calculations and graphical analyses were performed on the MATLAB programming platform, which provided an advanced digital computing environment. The optical and thermal properties of the tissue model were assumed to be independent of temperature changes. To accurately model the distribution of absorbed radiation in the tissue layers, the required unit-weighted total photon number, depending on the spatial resolution in the simulation, was used as one million. Body temperature was fixed to  $37^\circ\text{C}$  during all simulations. In addition, simulations can be improved to produce more accurate results by adding diffraction-limited beam diameter calculations.

Two simulation studies were performed. First, the situation in which the probe slides in a direction at a constant speed on the surface of the esophagus was simulated. In this simulation, the scanning speed was set to  $0.5\ \text{mm/s}$  on the x-axis. The total exposure time was 8 seconds. Continuous-wave laser radiation was ranged from 10 to 100 mW of power at a wavelength of  $1505\ \text{nm}$ . Figure 7 shows a representative example of the calculated distribution of photothermal damage in tissue volume at the end of 8 seconds IR laser exposure for all laser power sets. For example, this scan time corresponded to a total energy of  $0.8\ \text{J}$  at 100 mW laser power. The color bar indicates both the laser power and the estimated maximum injury depth at the end of the surface scan laser ablation.

In photothermal damage analysis, the generalized Arrhenius integral (Equation (2)) estimated the damage

**TABLE 1** Optical and thermal properties of tissue model used for photothermal mucosal ablation simulations

Parameters	Value
Reduced scattering coefficient ( $\mu_s'$ , $\text{cm}^{-1}$ )	9.5 [34]
Absorption coefficient ( $\mu_a$ , $\text{cm}^{-1}$ )	12 [34]
Refractive index ( $n$ )	1.32 [31]
Anisotropy factor ( $g$ )	0.6 [34]
Tissue density ( $\rho$ , $\text{kg/m}^3$ )	1126 [35]
Specific heat ( $C$ , $\text{J}\cdot\text{kg}^{-1}\cdot^\circ\text{C}^{-1}$ )	3720 [36]
Thermal conductivity ( $k$ , $\text{W}\cdot\text{m}^{-1}\cdot^\circ\text{C}^{-1}$ )	0.527 [35]
Frequency factor ( $\Lambda$ , $\text{s}^{-1}$ )	$1.3 \times 10^{95}$ [36]
Activation energy ( $E_a$ , $\text{J/mol}$ )	$6.04 \times 10^5$ [36]
Tissue thickness ( $t$ , $\text{mm}$ )	$<1.8$ [33]

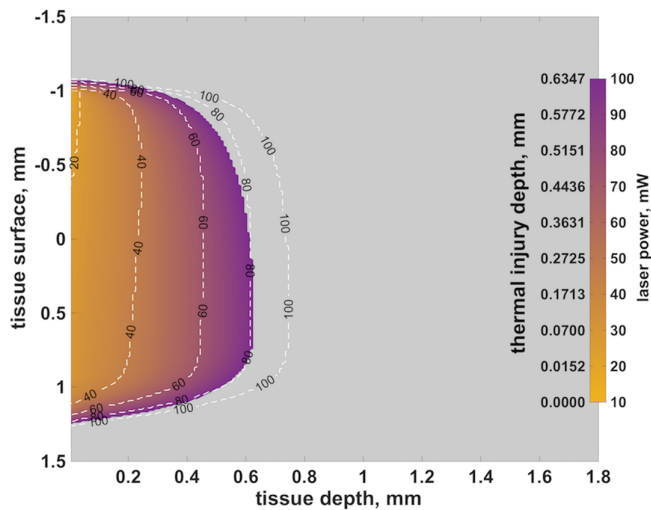


**FIGURE 7** Estimated cross-sectional frame of laser-induced thermal damage generated by the conical shaped fiber probe in the esophageal model (scan speed = 0.5 mm/s, ablation time = 8 seconds). On the other hand, the white dashed lines mark the estimated thermal injury depths produced by an 8.2- $\mu\text{m}$ -core fiber for comparison in the same laser power range and scanning speed

probability. A damage index ( $D$ ) of  $>0.99$  was used as the threshold for irreversible thermal damage. In regions with  $D > 0.99$ , the tissue was assumed to coagulate completely. The value of two rate process coefficients was derived from the literature [36]; frequency factor,  $\Lambda = 1.3 \times 10^{95}$  seconds<sup>-1</sup> and activation energy,  $E_a = 6.04 \times 10^5$  J/mol. The computer simulation successfully predicted that the peak temperature in the superficial tissue reached to  $100^\circ\text{C}$  (ie, the temperature sufficient to provide tissue vaporization) even at relatively low laser power (100 mW). More interestingly, the estimated thermal injury depths produced by a bare-ended single-mode fiber (8.2  $\mu\text{m}$  core diameter, non-chemically etched fiber) are shown in the same graph as the white dashed lines for direct comparison. The corresponding laser powers were also written in black on white dashed lines.

Second, the simulations in the first study were repeated for the 0.01 to 0.5 W laser power range at different scanning speeds to map the photothermal ablation depth as surface scanning speed and laser power matrix. The surface scanning speed varied from 0.5 to 5 mm/s on the x-axis (ie, tissue surface). Figure 8 shows the estimation of photothermal ablation depth as a function of surface scanning speed and laser power in color-coding format. The tissue vaporization threshold (the tissue temperature of  $\geq 100^\circ\text{C}$ ) level is highlighted as a solid white line on the map. As shown in Figure 8, it has been calculated that SPLA can be achieved by providing the total energy required to thermally damage the tissue during

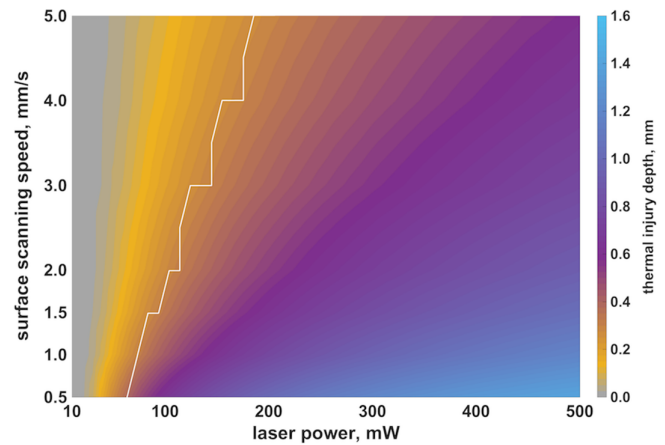


**FIGURE 8** A map of the estimated laser-induced thermal injury depth in the esophagus model as a function of the combination of surface scanning speed and laser power. The white solid line marks the tissue vaporization threshold (tissue temperature of  $\geq 100^\circ\text{C}$ )

slow surface scanning speeds with relatively low laser power.

The optical properties of the tissue at a particular wavelength define the depth of effective optical penetration within the tissue and thus the depth of the laser-induced thermal damage. Also, as expected, the build-up of residual thermal effects can expand the thermal injury depth over time. However, as shown in the photothermal ablation simulation results, the accumulation of sufficient thermal energy in the mucosa may be expedited for SPLA by decreasing laser power and increasing the exposure time (ie, slower surface scanning speed) accordingly or vice versa. Furthermore, the results presented here suggest that such rapid divergence of the tightly focused laser beam within the tissue may contribute to the definition of the depth of thermal penetration (Figure 7). Since the spot diameter increases rapidly as a function of tissue depth, the power density can be reduced to a level that minimizes localized thermal effects.

### 3.3 | SPLA of sheep esophagus

To investigate the feasibility of photothermal mucosal tissue ablation using a cone-shaped fiber probe and evaluate its technical performance, thermal injury studies were performed on ex vivo sheep esophagus. Figure 9 shows a representative example of visible thermal damage observed on the surface of the esophagus. The tissue sample was irradiated at a laser power of 400 mW in CW mode, corresponding to an irradiance of  $31.8 \times 10^5$  W/cm<sup>2</sup> for the 4- $\mu\text{m}$  beam diameter (estimated). The fiber tip was scanned at a constant speed of 1 mm/s on a single axis

over the tissue surface. The scan length was measured to be  $>0.4$  cm after a total ablation time of 4 seconds. Before laser ablation, the tissue surface was made as flat as possible with a small metal spatula.

In the assessment of the cellular thermal damage and thermal injury depth, an oxidoreductases group thermobile ( $>60^{\circ}\text{C}$ ) enzyme called lactate dehydrogenase (LDH) was labeled using NBT staining. The histologic marker of thermal damage was evaluated as follows: Staining was

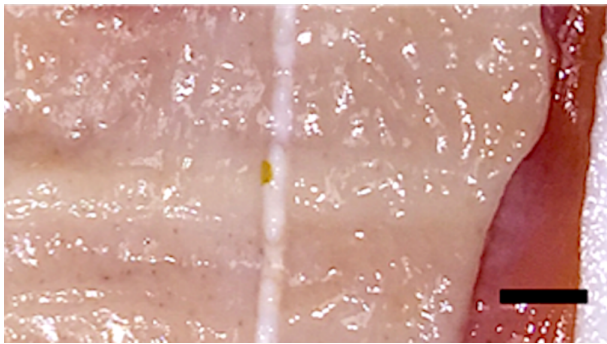


**FIGURE 9** Photograph of visible thermal damage after laser irradiation of sheep esophagus, ex vivo (wavelength = 1505 nm, laser power = 400 mW, surface scanning speed = 1 mm/s, ablation time = 4 seconds). Scale bar = 1 mm

associated with classical histology for heat-induced tissue damage, while dark blue indicated LDH positive as untreated normal esophageal tissue. Magnified images of NBT-stained fresh-frozen sheep esophagus samples are shown in Figure 10. The thickness of the histological tissue slices was  $12\ \mu\text{m}$ . Figure 10A represents an example of the microscopic image of the NBT-stained intact esophagus tissue as a control group to compare and assess the effect of the photothermal intervention. The relative distribution of the dark blue color over the histological section indicated that there was no thermal damage to the cellular structure during tissue processing.

Subsequently, laser ablation was performed for a constant surface scanning speed by varying the laser power at 50 mW intervals in the range of 300 to 450 mW. The scanning speed was set to 1 mm/s and the total laser exposure time was 6 seconds, corresponding to a scanned length of 6 mm. The bottom panels (B, C, D, E) of Figure 10 show cross-sectional injury profiles for respective laser power. High laser power induced uncontrolled large injury areas in the lateral sides; while all power settings generated enough energy to cause a detectable superficial (ie, mucosa and submucosa layers) injury in the NBT stained sections as shown. In particular, laser power settings of 300 and 350 mW provided a depth of

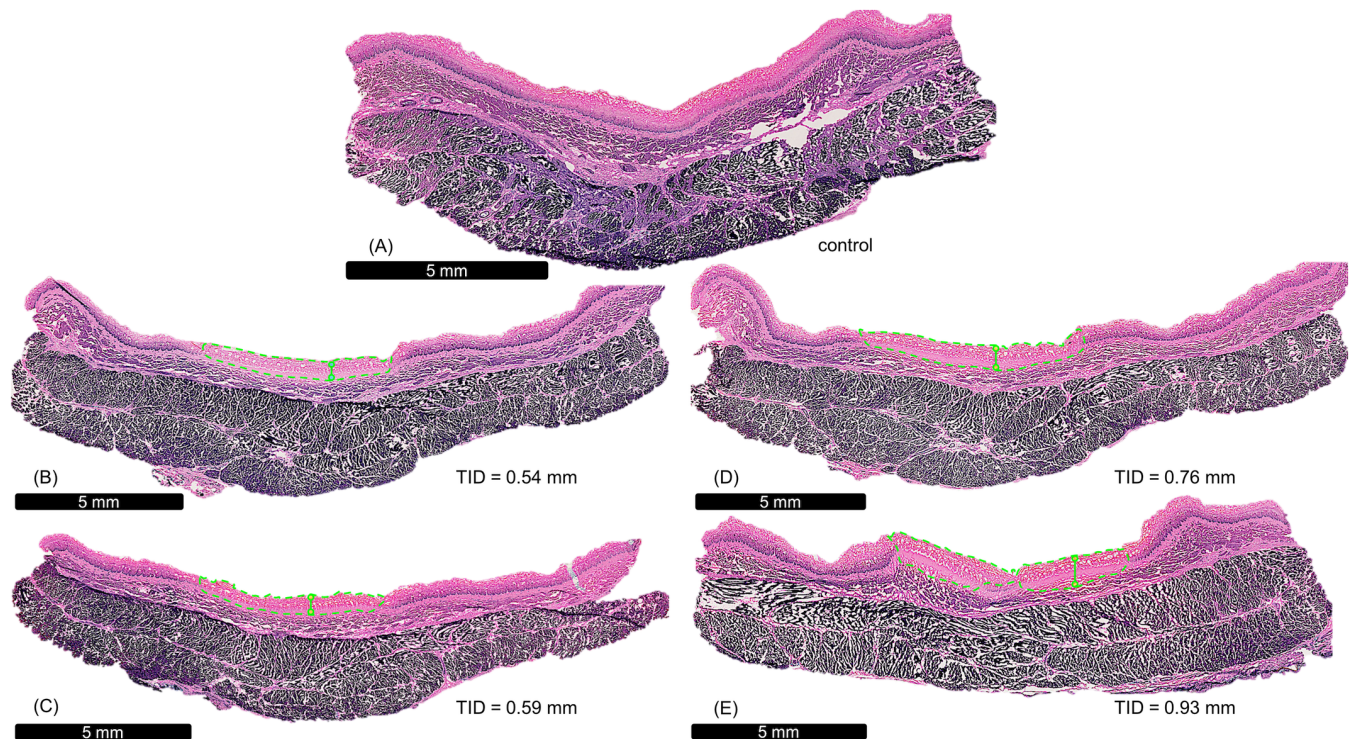


**FIGURE 10** Microscopy images of ex vivo sheep esophagus that were stained with nitroblue tetrazolium chloride. A, An intact ex vivo sheep esophagus as control, while other panels show the results of superficial photothermal laser ablation (SPLA) for laser power of 300 mW, B, 350 mW, C, 400 mW, D, and 450 mW, E. The measured thermal injury depths were approximately 0.54, 0.59, 0.76, and 0.93 mm, respectively. The surface scanning speed was set to 1 mm/s and the total scanning time was 6 seconds. TID, thermal injury depth

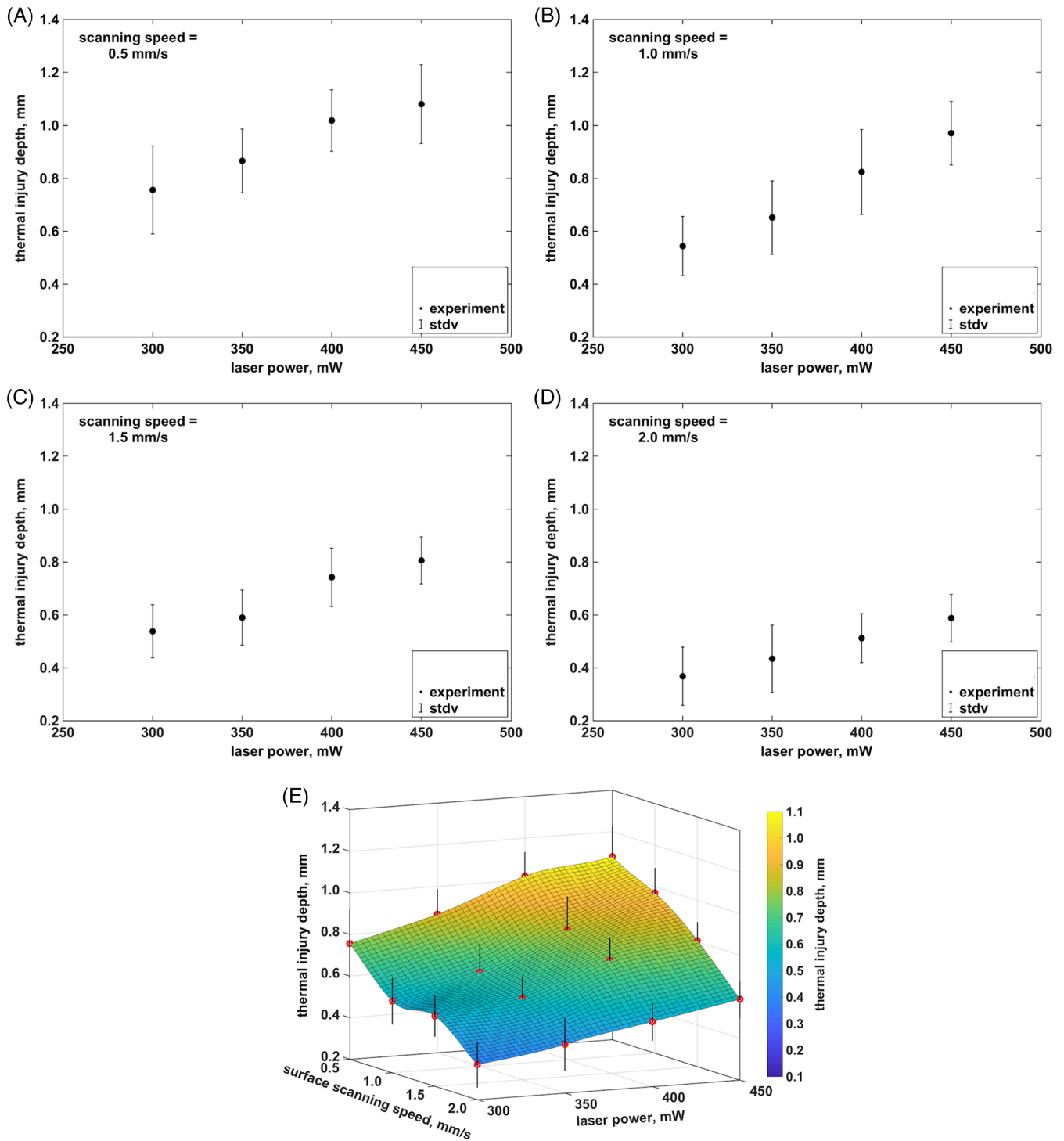


**FIGURE 11** Experimental measurements of laser-induced thermal injury depths performed for various combinations of surface scanning speed and laser power in ex vivo sheep esophagus model. These combinations included scanning speeds of 0.5 mm/s, A, 1 mm/s, B, 1.5 mm/s, C, and 2 mm/s, D, and laser power of 300, 350, 400, and 450 mW. E, Experimental measurements of cubic spline interpolation fittings in a three-dimensional plot. The red circles represent the mean values of thermal injury depth measurements, and the black lines indicate the SD for these measurements. A minimum of five laser ablation was conducted on ex vivo sheep esophagus at each laser incident power level (in ~50 mW increments)

thermal effect that would cause ablation at the first 0.6 mm depth, which was mainly associated with the mucosa layer [31]. On the other hand, as shown in

Figure 10E, irregularities in the depth of photothermal damage were also recorded. This may have two main reasons: (a) the difficulty in ensuring that the distance

between the probe and the surface remains constant across the tissue surface and (b) relatively short working distance provided by the cone-shaped fiber probe.

As a complementary study, experimental measurements of laser-induced thermal injury depths were performed for various combinations of surface scanning speed and laser power. These combinations included scanning speeds of 0.5, 1, 1.5 and 2 mm/s and laser power of 300, 350, 400, and 450 mW. A minimum of five laser ablation was conducted on ex vivo sheep esophagus at each laser incident power level (in ~50 mW increments) to demonstrate reproducibility.

Figure 11A-D shows thermal injury depth measurements with SD as a function of laser power for each surface scanning rate, respectively. Figure 11E demonstrates experimental measurements in a three-dimensional plot. The red circles represent the mean values of thermal injury depth measurements, and the black lines indicate the SD for these measurements. Besides, the surface graphs plot cubic spline interpolation fittings to experimental data. The three-dimensional plot is linked to a colormap ranging from 0.4 to 1.1 mm of the measured depth of injury. The calculated SD varies with speed-power combinations. In general, this high margin of error can be explained by local differences in tissue samples and their inhomogeneity, as well as the very short working distance provided by the cone-shaped fiber probe.

## 4 | DISCUSSION AND CONCLUSION

Prevention of the unintended consequences of BE endoscopic thermal therapy, such as organ narrowing, bleeding, or perforation, has been challenging because of the combination of deep thermal damage depth and multiple therapy sessions. Hence, the presence of effective endoscopic approaches that specifically provide a confined depth of thermal injury on the lining layer is still attractive in the treatment of BE. For example, studies using optical coherence tomography (OCT) technology have suggested to continuously measure or image the depth of the RF thermal effect to avoid further damaging to deep tissue layers [37, 38]. However, existing RF ablation probes developed for use only with white light endoscopic imaging completely conceal the area under treatment for OCT imaging [15, 39]. This allows OCT imaging of tissues before and after treatment, or only OCT imaging of local points.

In this context, it may be of interest to implement fiber-based probes that can form a fiber optic basis for real-time optical imaging during photothermal ablation therapy. More interestingly, fiber-based probe

approaches that enhance the superficial effect of photothermal therapy of mucosal tissue may aid in minimally destructive deeper tissue injury in a single-session therapy, and may result in improved postoperative patient quality-of-life.

This preliminary study investigates the feasibility of a cone-shaped fiber probe that provides continuous-wave IR laser radiation for SPLA in an ex vivo sheep esophageal model. A cone-shaped fiber tip was obtained with the chemical etching technique previously examined for various fiber optic applications, including optical trapping [40] and photocoagulation [41]. In summary, we have designed, built, and tested a fiber probe that provides a tightly focused laser beam at close range for high-efficiency photothermal ablation. The prototype probe allowed the use of relatively low laser power for a high-temperature rise in the superficial tissue, while also accumulating sufficient energy to thermally damage the mucosa layer of the sheep esophagus, ex vivo.

However, several limitations should be discussed in this preliminary feasibility study. First, the Arrhenius integral is generally and predominantly used to characterize thermal damage to biological tissue using direct protein denaturation measurements with increased scattering. On the contrary, it should be noted that this rate formulation does not take into account the nonlinear response of the tissue to laser-induced thermal effects.

Second, a more accurate beam diameter analysis is required to determine the beam diameter and focal length produced by the fiber probe. Such a high-focus laser beam provided by the cone-shaped fiber probe can be measured employing a high-resolution laser beam profiler or knife-edge method using a high precision photodetector with low ripple.

Third, the tip of the single-mode fiber probe becomes more fragile after chemical etching. Furthermore, the probe with a chemically etched fiber produces a relatively narrow area ( $\sim 1.3 \times 10^{-11} \text{ m}^2$ ) of ablation on the tissue surface at one time. Therefore, it is important and necessary to investigate a more suitable design that can combine a cone-shaped fiber bundle with a capsule that provides a recessed area and slides along the esophageal surface to cover a large region. In this way, the design may allow SPLA while avoiding short working distance and sensitive surface scanning issues.

Forth, the depth of local superficial therapy, which can be fixed by the rapid focus of the laser beam at the optimized wavelength, does not necessarily correlate to an anatomical landmark. Furthermore, the thickness of the mucosa layer may vary significantly from one patient to another. On the other hand, laser ablation of large surfaces (>2 cm in length) with a small diameter laser beam will take considerably longer in terms of treatment time.

This may limit the control of the therapy depth due to residual thermal effects.

Finally, a more rigorous histological analysis of thermal damage to the mucosa layer combined with an in vivo animal model is required to determine an optimal therapeutic window for consistent and reliable photothermal mucosa ablation using presented probe.

Our preliminary results presented in this article have demonstrated that the cone-shaped fiber probe using 1505-nm IR laser radiation is capable of providing both superficial and highly effective photothermal mucosa ablation of the sheep esophagus, ex vivo. This probe approach with further development may hold promise for endoscopic therapy of targeted-lining areas during a single-session procedure. More interestingly, with our technology, it may be possible to extend the same concept to other endoscopy therapy applications such as colon polyps.

## ACKNOWLEDGMENTS

The author thanks Merve Turker Burhan at Dokuz Eylul University for her help in generating some figures. The author also appreciates Dr Alper Bagriyanik at Dokuz Eylul University for his help in the histology analysis. This work was supported partially by TÜBİTAK grant No. 117E985, and the European Union's Horizon 2020 Research and innovation programme under the Marie Skłodowska-Curie grant agreement No. 835907. S.T. was supported by the Turkish Academy of Sciences Young Scientists Award Programme (2018 TÜBA-GEBIP).

## CONFLICT OF INTEREST

The authors declare no potential conflict of interest.

## ORCID

Serhat Tozburun  <https://orcid.org/0000-0002-4397-4011>

## REFERENCES

- [1] N. R. Barrett, *Surgery* **1957**, *41*, 881.
- [2] S. J. Spechler, R. K. Goyal, *Gastroenterology* **1991**, *110*, 614.
- [3] P. C. Enzinger, R. J. Mayer, *N. Engl. J. Med.* **2003**, *349*, 2241.
- [4] L. S. Engel, W. H. Chow, T. L. Vaughan, M. D. Gammon, H. A. Risch, J. L. Stanford, J. B. Schoenberg, S. T. Mayne, R. Dubrow, H. Rotterdam, A. B. West, M. Blaser, W. J. Blot, M. H. Gail, J. F. Fraumeni Jr., *J. Natl. Cancer Inst.* **2003**, *95*, 1404.
- [5] T. W. Rice, V. W. Rusch, C. Apperson-Hansen, M. S. Allen, L. Q. Chen, J. G. Hunter, K. A. Kesler, S. Law, T. E. Lerut, C. E. Reed, J. A. Salo, W. J. Scott, S. G. Swisher, T. J. Watson, E. H. Blackstone, *Dis. Esophagus* **2009**, *22*, 1.
- [6] J. Ronkainen, P. Aro, T. Storskrubb, S. E. Johansson, T. Lind, E. Bolling-Sternevald, M. Vieth, M. Stolte, N. J. Talley, L. Agréus, *Gastroenterology* **2005**, *129*, 1825.
- [7] K. M. Fock, T. L. Ang, *Expert Rev. Gastroenterol. Hepatol.* **2011**, *1*, 123.
- [8] M. Toruner, I. Soykan, A. Ensari, I. Kuzu, C. Yurdaydin, A. Ozden, *J. Gastroenterol. Hepatol.* **2004**, *19*, 535.
- [9] B. Odemiş, B. Çiçek, N. I. Zengin, M. Arhan, S. Kacar, C. Cengiz, O. Yüksel, *Dis. Esophagus* **2009**, *22*, 649.
- [10] G. D. De Palma, *World J. Gastroenterol.* **2012**, *18*, 6216.
- [11] R. Badillo, D. Francis, *World J. Gastrointest. Pharmacol. Ther.* **2014**, *5*, 105.
- [12] S. Seewald, T. L. Ang, N. Soehendra, *Postgrad. Med. J.* **2007**, *83*, 367.
- [13] J. K. Lee, R. Enns, *Can. J. Gastroenterol.* **2007**, *21*, 151.
- [14] N. J. Shaheen, G. W. Falk, P. G. Iyer, L. B. Gerson, *Am. J. Gastroenterol.* **2016**, *111*, 30.
- [15] D. E. Fleischer, V. K. Sharma, *Dig. Dis.* **2008**, *26*, 280.
- [16] M. C. Vassiliou, D. von Renteln, D. C. Wiener, S. R. Gordon, R. I. Rothstein, *Surg. Endosc.* **2010**, *24*, 786.
- [17] L. H. Alvarez, F. G. van Vilsteren, R. E. Pouw, F. J. W. ten Kate, M. Visser, C. A. Seldenrijk, H. M. I. van Berge Henegouwen, P. Fockens, B. L. Weusten, J. J. Bergman, *Gastrointest. Endosc.* **2011**, *73*, 682.
- [18] A. C. Strauss, A. T. Agoston, P. S. Dulai, A. Srivastava, R. I. Rothstein, *Surg. Endosc.* **2014**, *28*, 3366.
- [19] T. Dix, H. Barr, *Laser Applications in Medicine and Dentistry*, Vol. 1922, SPIE, Vienna **1996**, p. 275.
- [20] J. A. Salo, J. T. Salminen, T. A. Kiviluoto, A. T. Nemlander, O. J. Rämö, M. A. Färkkilä, E. O. Kivilaakso, S. P. Mattila, *Ann. Surg.* **1998**, *227*, 40.
- [21] H. Barr, N. Stone, B. Rembacken, *Gut* **2005**, *54*, 875.
- [22] M. Vieth, L. Mastracci, N. Vakil, J. Dent, B. Wernersson, I. Baldycheva, J. Wissmar, M. Ruth, R. Fiocca, *Clin. Gastroenterol. Hepatol.* **2016**, *14*, 1544.
- [23] S. Mononobe, M. Ohtsu, *J. Light. Technol.* **1996**, *14*, 2231.
- [24] B. A. F. Puygranier, P. Dawson, *Ultramicroscopy* **2000**, *85*, 235.
- [25] L. Wang, S. L. Jacques, L. Zheng, *Comput. Methods Programs Biomed.* **1995**, *47*, 131.
- [26] F. C. Henriques, A. D. Moritz, *Am. J. Pathol.* **1947**, *23*, 582.
- [27] J. B. Liu, L. S. Miller, B. B. Goldberg, R. I. Feld, A. A. Alexander, L. Needleman, D. O. Castell, P. J. Klenn, C. L. Millward, *Radiology* **1992**, *184*, 721.
- [28] D. K. Taniguchi, R. W. Martin, E. A. Trowers, F. E. Silverstein, *Gastrointest. Endosc.* **1995**, *41*, 582.
- [29] T. M. Glanzmann, M. P. Zellweger, F. Borle, R. Conde, A. Radu, J. P. Ballini, Y. Jaquet, R. Pilloud, H. Bergh, P. Monnier, S. Andrejevic-Blant, G. A. Wagnieres, *Lasers Surg. Med.* **2009**, *41*, 643.
- [30] A. Radu, R. Conde, C. Fontolliet, G. Wagnieres, H. Berg, P. Monnier, *Gastrointest. Endosc.* **2003**, *57*, 897.
- [31] G. M. Hale, M. R. Querry, *Appl. Optics* **1973**, *12*, 555.
- [32] B. E. A. Saleh, M. C. Teich, *Fundamentals of Photonics*, John Wiley & Sons, New York **1991**, Ch. 8.
- [33] M. Hohmann, B. Lengenfelder, R. Kanawade, F. Klämpfl, A. Douplik, H. Albrecht, *J. Biophotonics* **2018**, *11*, 1.
- [34] A. N. Bashkatov, E. A. Genina, I. V. Kochubey, A. A. Gavriloa, S. V. Kapralov, V. A. Grishaev, V. V. Tuchin, *Med. Laser Appl.* **2007**, *22*, 95.
- [35] C. M. Collins, M. B. Smith, R. Turner, *J. Appl. Physiol.* **2004**, *97*, 2051.
- [36] K. R. Diller, G. A. Klutke, Proceedings of the 1993 ASME Winter Annual Meeting, ASME, New Orleans, LA, **1993**, 268, 117.

- [37] H. C. Lee, O. O. Ahsen, J. J. Liu, T.-H. Tsai, Q. Huang, H. Mashimo, J. G. Fujimoto, *J. Biomed. Opt.* **2017**, *22*, 076001.
- [38] W. C. Y. Lo, N. Uribe-Patarroyo, K. Hoebel, K. Beaudette, M. Villiger, N. S. Nishioka, B. J. Vakoc, B. E. Bouma, *Biomed. Opt. Express*. **2019**, *10*, 2067.
- [39] B. J. Dunkin, J. Martinez, P. A. Bejarano, C. D. Smith, K. Chang, A. S. Livingstone, W. S. Melvin, *Surg. Endosc.* **2006**, *20*, 125.
- [40] J. B. Decombe, S. Huant, J. Fick, *Opt. Express* **2013**, *21*, 30521.
- [41] V. G. Truong, S. Park, V. N. Tran, H. W. Kang, *Biomed. Opt. Express* **2017**, *8*, 5663.

**How to cite this article:** Tozburun S. Superficial photothermal laser ablation of ex vivo sheep esophagus using a cone-shaped optical fiber tip. *J. Biophotonics*. 2020;13:e201960116. <https://doi.org/10.1002/jbio.201960116>